molecules

MDPI

Review

New Horizons in Chemical Functionalization of Endohedral Metallofullerenes

Michio Yamada [1,*], Michael T. H. Liu [2], Shigeru Nagase [3] and Takeshi Akasaka [1,4,5,6,*]

1 Department of Chemistry, Tokyo Gakugei University, Koganei, Tokyo 184-8501, Japan
2 Department of Chemistry, University of Prince Edward Island, Charlottetown, PE C1A4P3, Canada; diazirine@gmail.com
3 Fukui Institute for Fundamental Chemistry, Kyoto University, Sakyo-ku, Kyoto 606-8103, Japan; nagase@ims.ac.jp
4 TARA Center, University of Tsukuba, Tsukuba, Ibaraki 305-8577, Japan
5 Foundation for Advancement of International Science, Tsukuba, Ibaraki 305-0821, Japan
6 State Key Laboratory of Materials Processing and Dye and Mold Technology, School of Materials Science and Engineering, Huazhong University of Science and Technology, Wuhan 430074, China
* Correspondence: myamada@u-gakugei.ac.jp (M.Y.); akasaka@tara.tsukuba.ac.jp (T.A.); Tel.: +81-(0)42-329-7493 (M.Y.)

Academic Editors: Burgert Blom, Erika Ferrari, Vassilis Tangoulis, Cédric R Mayer, Axel Klein and Constantinos C. Stoumpos
Received: 20 June 2020; Accepted: 6 August 2020; Published: 10 August 2020

Abstract: This overview explains some new aspects of chemical functionalization of endohedral metallofullerenes (EMFs) that have been unveiled in recent years. After differences in chemical reactivity between EMFs and the corresponding empty fullerenes are discussed, cage-opening reactions of EMFs are examined. Then, the selective bisfunctionalization of EMFs is explained. Finally, single-bonding derivatization of EMFs is addressed. The diversity and applicability of the chemical functionalization of endohedral metallofullerenes are presented to readers worldwide.

Keywords: addition reactions; carbenes; chemical functionalization; electrochemistry; endohedral metallofullerene; fullerene; lanthanide ions; nanocarbon; pericyclic reactions; radicals

1. Introduction

Endohedral metallofullerenes (EMFs) are hybrid molecules of spherical nanocarbons, known as fullerenes, with atomic metal(s) or metal-containing clusters encaged inside. Unique molecular structures of this kind have fascinated many researchers in many fields, including chemistry, physical science, and materials science. Soon after the discovery of C_{60}, EMFs were first reported in 1985 by Smalley and coworkers [1]. Findings from early studies of their synthesis, structures, and properties were summarized in several reports [2–5]. In addition, research progress after 2010 has been described in several published reviews [6–13]. Recent progress on silylation and germylation of EMFs was reviewed by Kako et al. [14] However, several chemical reactions of EMFs have been developed since. Various molecular structures of EMF derivatives have been clarified one after another. This review was undertaken to overview the most recent advances in the chemistry of EMFs developed in the last decade, particularly addressing chemical functionalization.

2. Differences in Chemical Reactivity between EMFs and the Corresponding Empty Fullerenes

The chemical reactivities of EMFs differ from those of empty fullerenes, because of their different carbon-cage geometries and their different redox properties. Comparison of the chemical reactivities of EMFs with those of empty fullerenes is expected to provide deeper understanding of how endohedral metal-atom doping affects the chemical reactivity of fullerenes. However, the difficulty of pursuing

this subject experimentally is that most carbon cages of EMFs are not available in their pristine forms. Empty fullerenes and EMFs are synthesized, generally by arc-discharging of graphitic carbon containing metal species such as metal oxides. Because of the intense temperature (2000–3000 K) conditions, the resulting fullerene species are regarded not as kinetically but as thermodynamically favorable ones. At this point, the presence or absence of 'intramolecular' electron transfer from the inner metal atom(s) to the outer carbon cages drastically alters the thermodynamic stability of the carbon cages. For instance, adjacent pentagonal rings are disfavored in the carbon cages of empty fullerenes. Therefore, empty fullerenes generally satisfy the empirical rule, the so-called isolated pentagon rule (IPR), which states that stable fullerenes have each of their 12 pentagonal rings surrounded by five hexagonal rings [15]. In fact, fusing pentagonal rings increases the local steric strain caused by enforced bond angles, accompanied by the higher pyramidalization of the carbon atoms. In addition, a fused pentagon substructure must be antiaromatic. Nonetheless, the circumstances are different in the case of EMFs [16]. In fact, several EMFs that possess non-IPR carbon cages have been discovered to date [17]. Crystallographic studies of such non-IPR EMFs clearly illustrate that the encaged metal atoms are closely positioned near the fused pentagonal rings on the carbon cages, implying that the encaged metal atoms stabilize the non-IPR carbon cages that are not available in pristine forms without encaged metal atoms. As a result, studies using experimentation to compare the chemical reactivities of empty fullerenes and the EMFs were left unexplored until 2016.

In this respect, we have specifically examined on the D_{2d}(23)-C_{84} carbon cage, because the carbon cage is the sole exception by which both the empty and the endohedral species are thermodynamically stable at ambient conditions. The empty fullerene was first reported in 1992 by Kikuchi, Achiba, and their coworkers [18]. Its isolation was reported by Dennis and Shinohara in 1998 [19]. As indicated in its name, D_{2d}(23)-C_{84} has the molecular symmetry of D_{2d}; it, therefore, consists of the 11 nonequivalent carbon atoms. The number in the parenthesis indicates the spiral code for IPR-satisfying cage structures assigned based on the Fowler–Manolopoulos (FM) spiral algorithm, which is used to designate the cage structure [20]. The corresponding EMF, which contains the same carbon cage, Sc_2C_2@D_{2d}(23)-C_{84}, was first reported by Shinohara et al. However, it was assigned incorrectly at that time as Sc_2@C_{86} [21]. The correct structure of the EMF as Sc_2C_2@D_{2d}(23)-C_{84} was revised by the same group, based on the maximum entropy method (MEM)/Rietveld analysis of the powder X-ray diffraction data [22]. The revised structure was finally confirmed by Akasaka et al., based on two-dimensional incredible natural abundance double quantum transfer experiment (2D INADEQUATE) NMR studies of its ^{13}C-enriched sample [23]. The 'molecular' symmetry of Sc_2C_2@D_{2d}(23)-C_{84} can be regarded not as D_{2d}, but as C_{2v}. Lowering of the molecular symmetry results from the placement of the internal Sc_2C_2 cluster, by which the C_2 unit is not parallel but rather perpendicular to the main C_2 axis. Nevertheless, the lower availability of both the species hampered further studies of their chemical reactivities.

We launched a large-scale arc-discharge chamber and optimized both the discharging conditions and the extraction–purification processes, to obtain sufficient amounts of such 'minor' fullerene products [8]. Subsequently, we conducted experiments that revealed differences in the chemical reactivity and selectivity between D_{2d}(23)-C_{84} and Sc_2C_2@D_{2d}(23)-C_{84} (hereinafter, the molecules will be abbreviated respectively as C_{84} and Sc_2C_2@C_{84}), for which the photo-reactions of the fullerenes with 2-adamantane-2,3′-[3*H*]-diazirine (**1**) were used for the investigation, as shown in Figure 1 [24]. The photolysis of **1** is well known to generate both adamantylidene carbene Ad: (Ad = adamantylidene) and diazoadamantane as reactive intermediates in a 1:1 ratio, based on laser flash photolysis studies [25]. The photo-reaction of C_{84} and **1** at ambient temperature caused the formation of two mono-adducts, major product **2a** and minor product **2b**, for which the respective conversion yields of **2a** and **2b** based on the reacted C_{84} were 80% and 12% (see Figure 1a). In that case, 52% of C_{84} was consumed during 90 s irradiation using an ultra-high-pressure mercury-arc lamp (cutoff < 350 nm). The **2a** and **2b** structures were assigned respectively to the [5,6]-(a–b)-open fulleroid and the [6,6]-(a–a)-closed methanofullerene, for which the terms [5,6] and [6,6] respectively show that the site of addition occurred at a bond shared by one pentagonal ring and one hexagonal ring, or a bond shared by two hexagonal rings. The structure

of **2b** was also ascertained using single-crystal XRD. No interconversion was observed between **2a** and **2b** under photoirradiation. However, **2a** was thermally interconverted to **2b** under heating at 80°C.

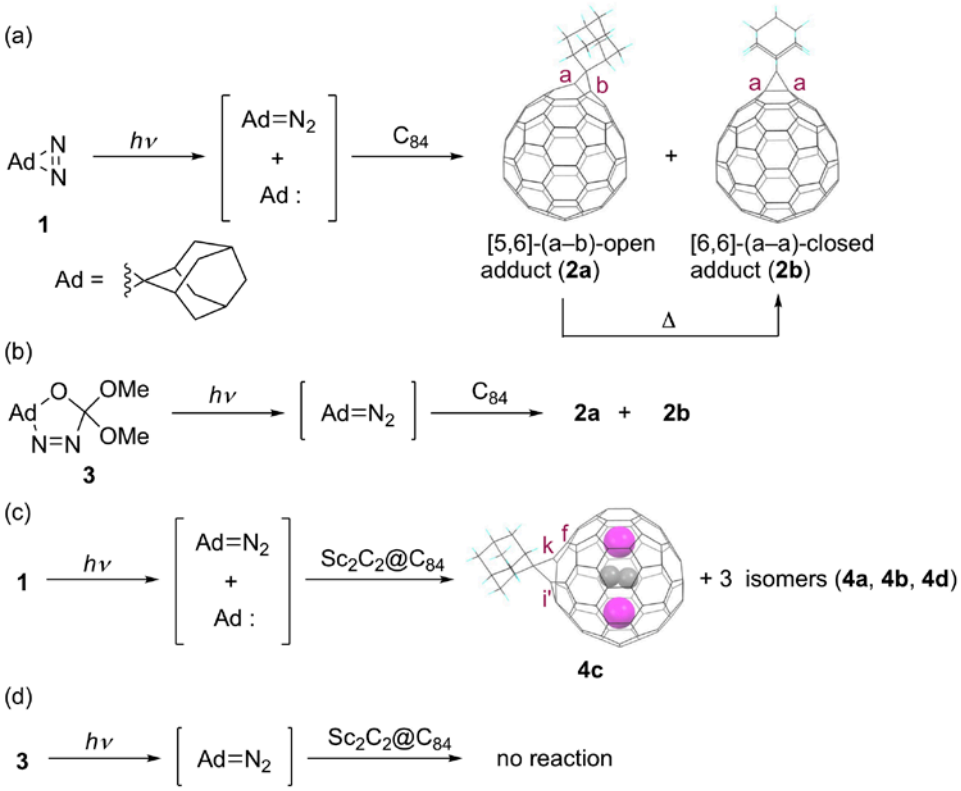

Figure 1. (**a**) Photochemical reaction of C_{84} and **1**. (**b**) Photochemical reaction of C_{84} and **3**. (**c**) Photochemical reaction of $Sc_2C_2@C_{84}$ and **1**. (**d**) Photochemical reaction of $Sc_2C_2@C_{84}$ and **3**.

To assess the chemical reactivity of C_{84} toward the reactive intermediates, comparative studies of the photolysis of **1** and 5′.5′-dimethoxyspiro[adamantane]-2,2′-[Δ^3-1,3,4-oxadiazoline] (**3**) in the presence of C_{84} at –78°C were conducted, respectively, because **3** is known to generate diazoadamantane exclusively under photoirradiation (see Figure 1b). On one hand, the photoreaction of C_{84} with **1** caused the formation of **2a** and **2b** in a 10:1 ratio under the condition. On the other hand, the photoreaction of C_{84} with **3** caused the formation of **2a** and **2b** in a ratio of 10:1, which is the same ratio as that obtained in the reaction of C_{84} and **1**. The comparable product ratios imply that in situ generated diazoadamantane contribute mainly to the reaction process in the photolysis of **1** in the presence of C_{84}. Combined with density functional theory (DFT) calculations, the scenario of the photoreactions was proposed as follows: first, the regioselective [3 + 2] cycloaddition of C_{84} with in-situ generated diazoadamantane took place at the [6,6]-(a–a) bond, in which the two-fold degenerate LUMO is localized primarily, to give the pyrazoline intermediate. Secondly, thermal decomposition of the pyrazoline intermediate occurred in a concerted pathway, to give **2** exclusively. Finally, a concerted [1,5]-sigmatropic shift of **2a** led to the formation of **2b**.

In contrast to that of the empty fullerene, the photoreaction of $Sc_2C_2@C_{84}$ with **1** at ambient temperature yielded four monoadducts, **4a**, **4b**, **4c**, and **4d** in an 8:7:3:1 ratio, respectively, after 1 min (see Figure 1c). Among these, only the structure of **4c** has been elucidated by single-crystal XRD, showing that the third most abundant isomer is the [6,6]-(k–i′)-open fulleroid. No interconversion was observed between **4a** and **4b** under photoirradiation, but they both interconvert to **4c** under thermal conditions. It is noteworthy that no reaction proceeded in the photolysis of **3** in the presence of $Sc_2C_2@C_{84}$, indicating that $Sc_2C_2@C_{84}$ is not reactive toward diazoadamantane (see Figure 1d). In this context, it is reasonable to consider that the photoreaction of $Sc_2C_2@C_{84}$ with **1** proceeded via a carbene

addition mechanism, unlike the corresponding empty fullerene. Unfortunately, an experiment on the structural elucidation of **4a**, **4b**, and **4d** has not been conducted. However, based on the hypothesis that the addend must move to bind with an adjacent bond during thermal interconversion and the DFT calculations of the relative energies, **4a** and **4b** can be the [6,6]-(k–k) and [6,6]-(k–f) addition products. Inspection of the molecular orbital (MO) diagrams shows that the LUMO of $Sc_2C_2@C_{84}$ is higher in energy than that of C_{84}. Therefore, the inertness of $Sc_2C_2@C_{84}$ toward diazoadamantane can be derived from the energy mismatch between their frontier orbitals. However, the higher level of the HOMO of $Sc_2C_2@C_{84}$ compared to that C_{84} might result in promoting reactivity toward the electrophilic carbene. Nevertheless, the delocalization of the HOMO of $Sc_2C_2@C_{84}$ hampers the proper prediction of the reactive sites. The addition sites of the proposed structures of **4a** and **4b**, and the XRD-determined structure of **4c** cannot be explained based either on the *p*-orbital axis vector (POAV) values or on the negative-charge densities. DFT calculations suggest that the formation of **4c** is governed by thermodynamic control. Throughout, their different chemical reactivities of C_{84} and $Sc_2C_2@C_{84}$ are derived from Sc_2C_2 doping, which raises the HOMO and LUMO levels of the carbon cage. The changes switch the reactivity in the photolysis of **1**.

3. Cage-Opening Reactions of EMFs

Among the various chemical functionalizations of fullerenes, cage-opening reactions are those which enable one to gain access to the inner space of the otherwise "locked" carbon sphere. Wudl and co-workers first introduced the concept that creates an orifice on the carbon cage in 1995 [26]. Since then, several examples of open-cage fullerenes prepared from C_{60} and C_{70} have been developed. A prominent result is the fact that the open-cage fullerenes that enable the encapsulation of small molecules such as H_2 [27,28], H_2O [29,30], HF [31,32], and even CH_4 [33] are available. Further orifice-closing reactions engender the creation of endohedral fullerenes. In contrast, cage-opening reactions of EMFs have remained unexplored until recently, due to the limited availability of EMFs and different chemical reactivities of EMFs from those of empty fullerenes. In 2011, Wang and coworkers found, by accident, that benzyne addition to $Sc_3N@I_h(7)$-C_{80} (hereinafter abbreviated as $Sc_3N@C_{80}$) yielded an oxygen-bridged open-cage EMF derivative **7** in addition to the [6,6]-benzyne adduct **5** and [5,6]-benzyne adduct **6**, when the reaction was conducted under air, as shown in Figure 2 [34]. Both **5** and **6** possess closed four-membered rings at the site of addition, which are formed through formal [2 + 2] cycloaddition of the in-situ generated benzyne to $Sc_3N@C_{80}$. The corresponding [4 + 2] cycloaddition does not occur because fullerenes do not act as dienes. The formation of **7** became dominant, when the reaction of $Sc_3N@C_{80}$ with 2-amino-4,5-diisopropoxybenzoic acid and isoamyl nitrite (reactant ratio: 1:5:8) was conducted in 1,2-dichlorobenzene (1,2-DCB) in the presence of 25 equiv. of water under aerobic conditions at 60°C for 12 h. Under these conditions, **5**, **6**, and **7** were obtained, respectively, in 7%, 3%, and 12% yields, in addition to the recovery of the pristine EMF in 46% yield. The single-crystal XRD studies of **7** revealed its unique molecular structure. First, the [5,6] C–C bond at the site of the benzyne addition is broken. Secondly, an oxygen atom was added to one of the [5,6] C–C bonds of the benzyne-attached pentagonal ring, in which the C–C bond is also broken to form not an epoxy, but an ether substructure on the cage. Consequently, the carbon cage of **7** contains a 13-membered ring orifice, although the orifice is spanned by an oxygen and a benzyne moiety. Presumably, **7** was formed by oxygenation of **6**, although details of the reaction mechanism for the formation of **7** remain unclear. In fact, both **5** and **6** were stable in air at 60°C for 12 h and at 180°C for 8 h.

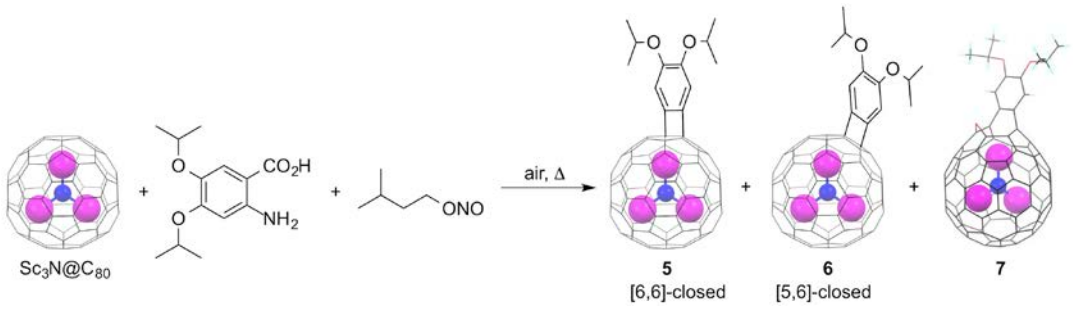

Figure 2. Cycloaddition reaction of $Sc_3N@C_{80}$ with 2-amino-4,5-diisopropoxybenzoic acid and isoamyl nitrite, to produce open-cage metallofullerene **7**.

To access the inner space of EMFs, no bridging moiety at the orifice is necessary. In this regard, an open-cage EMF bearing three seven-membered ring orifices without bridges was first reported in 2015 using $La_2@D_2(10611)$-C_{72} as the starting material, as shown in Figure 3 [35]. The dimetallofullerene $La_2@D_2(10611)$-C_{72}, known as a non-IPR EMF, contains two pentalene units at opposite ends of the rugby ball-shaped carbon cage [36]. In this context, exploration for the chemical functionalization of $La_2@D_2(10611)$-C_{72} (hereinafter, the molecule will be abbreviated as $La_2@C_{72}$) is also important for elucidating the chemical reactivity of non-IPR EMFs. As a cage-opening, the thermal reaction of $La_2@C_{72}$ with 5,6-diphenyl-3-(2-pyridyl)-1,2,4-triazine at 180°C in a sealed tube was conducted. After 72 h, 68% of $La_2@C_{72}$ was consumed, and it was converted quantitatively to two bisfulleroid isomers (labelled as **8a** and **8b**) in a 1:1 ratio. Between them, the single-crystal XRD analysis of **8a** revealed its open-cage structure. The results suggest that the initial [4 + 2] cycloaddition took place at the [5,5] C–C bond, at one of the two pentalene units. After N_2 extrusion, the subsequent electrocyclization and the following cycloreversion sequence produced the final open-cage structure. In this respect, the selective reaction at the [5,5] junction resulted from the highest reactivity of the central C–C bond of the pentalene units. However, the unique site selectivity of $La_2@C_{72}$ is not predictable based on the frontier orbital criteria. In fact, DFT calculations suggest that HOMO, LUMO+1, and LUMO+2 of $La_2@C_{72}$ are strongly delocalized over the whole sphere, whereas the LUMO is located mainly on the internal La atoms. Instead, the POAV values can be useful to explain the highest reactivity of the [5,5]-bond. The crystallographic determination of the molecular structure of **8b** is missing. However, it can be deduced that the first reaction step occurred at the same [5,5]-bond because the other diastereomer can be formed by the addition of the triazine to the bond in its reversed direction.

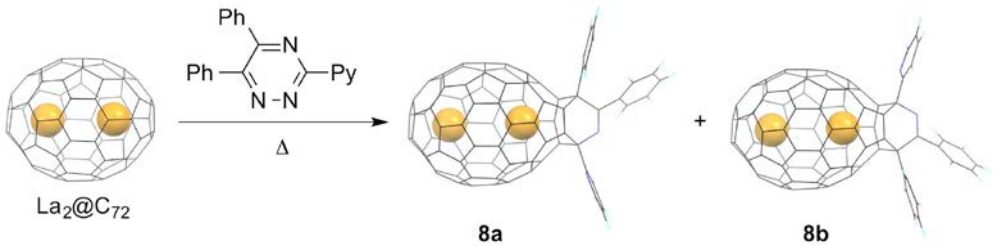

Figure 3. Cage-opening reaction of $La_2@C_{72}$ with 5,6-diphenyl-3-(2-pyridyl)-1,2,4-triazine.

4. Selective Bis-Addition Reactions of EMFs

It is reasonable to consider that the site selectivity of EMFs is influenced by the internal metal species, because the charge density distribution of the cage carbons and the frontier MO distribution of the whole molecule are changed drastically by metal doping [8]. For instance, in $La@C_{2v}(9)$-C_{82}, the La atom is localized near the hexagonal ring along the C_2 axis of the C_{2v} carbon cage. Consequently, the carbons close to the La atom are negatively charged, while, on the contrary, the carbons distant from the La atom are positively charged. As a result, electrophilic reactions tend to occur at the cage carbons close to the La atoms, whereas nucleophilic reactions tend to occur at the cage carbons at the

opposite side. In this regard, dimetallic EMFs are likely to be suitable reactants for selective bis-addition reactions. The first example of the bisadduct formation of dimetallic EMFs was the photochemical reaction of $La_2@C_{72}$ with **1** reported by our group in 2008 [37,38]. In this reaction, seven isomers of $La_2@C_{72}(Ad)_2$ (**9a**–**9g**) were isolated, of which the structure of the most abundant isomer **9a** was found using single-crystal XRD, as shown in Figure 4a. Results indicated that two Ad groups were added to the two pentalene regions at both poles of $La_2@C_{72}$, which face the encaged La atoms. Based on the high reactivity of the pentalene regions, the two Ad groups are likely to have added to the two poles in the other bisadduct isomers.

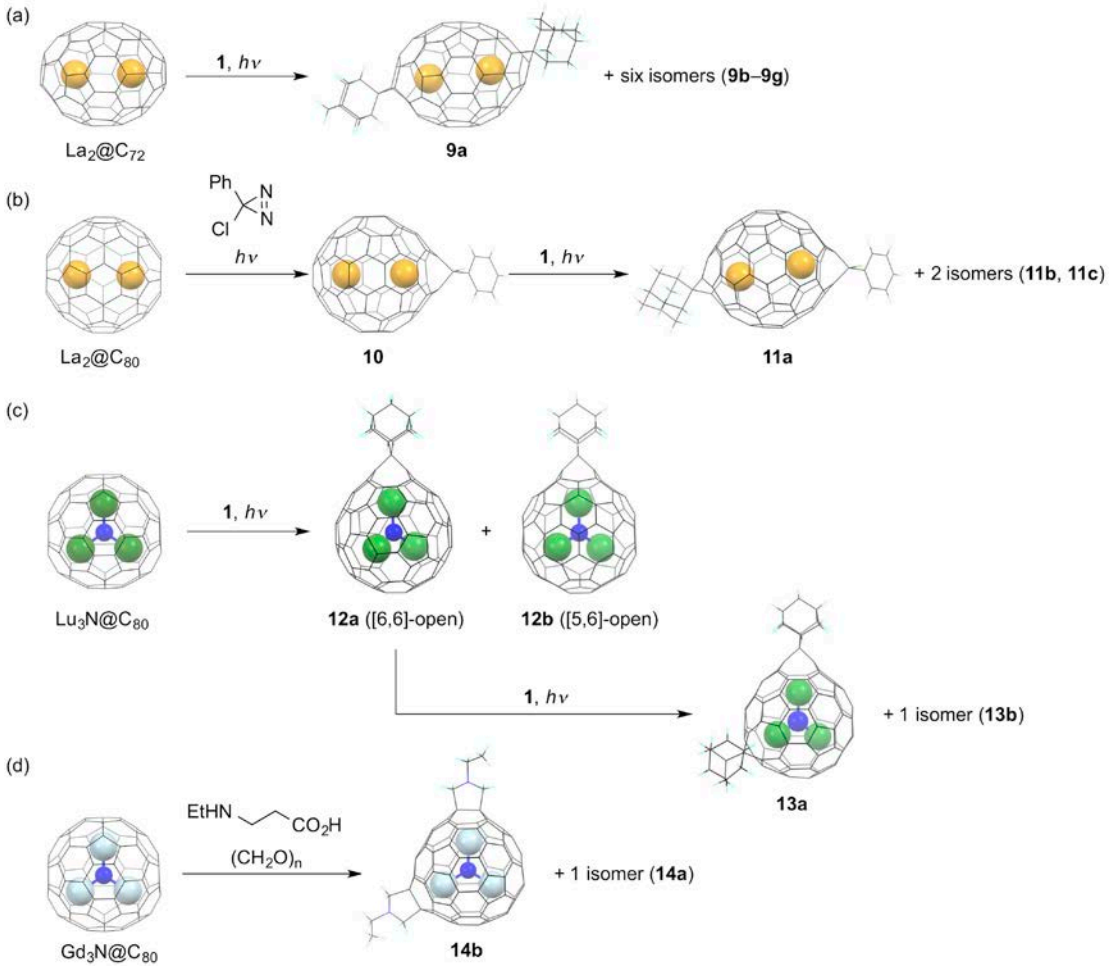

Figure 4. Bisfunctionalization of EMFs. (**a**) Photochemical reaction of $La_2@C_{72}$ and **1**. (**b**) Two-step bisfunctionalization of $La_2@C_{80}$. (**c**) Two-step bisfunctionalization of $Lu_3N@C_{80}$. (**d**) Prato reaction of $Gd_3N@C_{80}$ with *N*-ethylglycine and paraformaldehyde.

In contrast to the rugby-ball-shaped $La_2@C_{72}$ molecule, the selective bis-addition reaction of $La_2@I_h(7)$-C_{80} was not straightforward, due to its round structure and three-dimensional dynamic motion of the encaged La atoms [39]. At this point, a stepwise addition reaction protocol is an alternative pathway to obtain the corresponding bisadducts regioselectively [40]. As the first step, the photochemical reaction of $La_2@I_h(7)$-C_{80} with phenylchlorodiazirine was conducted, as shown in Figure 4b. The resulting monoadduct, [6,6]-open $La_2@I_h(7)$-C_{80}(CClPh) (**10**), features the two encaged La atoms collinear with the spiro carbon of the attached Ad moiety [41]. Regulation of the motion of the La atoms is attributable to the C–C bond breaking of the addition site, which engenders elongation of the La···La distance. As a result, the two La atoms are localized respectively at the position close to the addition site and the opposite side of the addition site. Therefore, the latter site is expected to be more reactive toward an electrophile. As the second step, the photochemical reaction of **10** with

1 proceeded smoothly to afford three isomers of the bisadduct $La_2@I_h(7)$-C_{80}(CClPh)(Ad) (**11a**–**11c**). One can notice that the second carbene addition afforded only three isomeric adducts, although many possible addition sites exist in **10**. Single-crystal XRD studies of **11a** have revealed that the two addends are attached to both ends of the $La_2@I_h(7)$-C_{80} molecule. The Ad addition coincided with the C–C bond cleavage at the site of addition. These studies indicate clearly that the encaged metal atoms in EMFs can regulate the reactive sites.

This is also in the case for trimetallic nitride-templated EMFs (TNT-EMFs). In early works, Gibson, Dorn, and coworkers reported that the Bingel–Hirsch reaction of $Sc_3N@D_{3h}(5)$-C_{78} with diethyl bromomalonate in the presence of DBU afforded a highly symmetrical bisadduct $Sc_3N@D_{3h}(5)$-$C_{78}[C(CO_2Et)_2]_2$, in addition to the monoadduct $Sc_3N@D_{3h}(5)$-$C_{78}[C(CO_2Et)_2]$ in 2008, although the addition site was not fully characterized [42]. In 2017, our group reported the first example for the X-ray crystallographic structure of a TNT-EMF bisadduct, as shown in Figure 4c [43]. In $Lu_3N@I_h(7)$-C_{80}, the encaged metal cluster exhibits three-dimensional random motion in the carbon sphere. Consequently, a stepwise strategy was adopted for regioselective bisfunctionalization. As the first step, the photochemical reaction of $Lu_3N@I_h(7)$-C_{80} with **1** afforded [6,6]-open $Lu_3N@I_h(7)$-C_{80}(Ad) (**12a**) as the major product, and [5,6]open $Lu_3N@I_h(7)$-C_{80}(Ad) (**12b**) as the minor product. The X-ray crystallographic structures of **12a** and **12b** disclosed that one metal site was positioned near the addition site. The other two Lu atoms were disordered and positioned at eight sites. The results indicated that the Lu_3N cluster is allowed to rotate similarly to a spinning top inside the carbon sphere. The subsequent photochemical reaction of the **12a** with **1** proceeded regioselectively to afford two bisadducts (**13a** and **13b**) that were isolated by subsequent HPLC separation. The X-ray structure of **13a** showed that the second Ad group was attached at a [6,6] bond near a Lu atom in a [6,6]-open fashion. Therefore, one can reasonably state that the regioselectivity in the Ad bisaddition is regulated by the triangular structure of the endohedral Lu_3N cluster. Actually, DFT calculations suggest that the X-ray determined bisadduct isomer is the most stable one among five candidates.

Later, Yamakoshi et al. reported the X-ray structure of a bis-ethylpyrrolidinoadduct of $Gd_3N@I_h(7)$-C_{80} (hereinafter, the molecule is abbreviated as $Gd_3N@C_{80}$) prepared by 1,3-dipolar cycloadditions (so-called Prato reaction [44–49]) of $Gd_3N@I_h(7)$-C_{80}, with excess amounts of *N*-ethylglycine and paraformaldehyde in 2019 [50]. The reaction yielded two isomers of the bisadducts (**14a** and **14b**), in addition to the corresponding monoadduct, as shown in Figure 4d [51]. The crystal structure of the minor isomer **14b** exhibited a C_2-symmetric [6,6][6,6]-structure. The addition sites of the minor isomer of $Gd_3N@I_h(7)$-$C_{80}[(CH_2)_2NEt]_2$ differ from those of **13a**, even though two of the three Gd atoms of the internal Gd_3N cluster are positioned close to the sites of the additions, as expected. The Gd_3N cluster was flattened out in the crystal structure of the minor bisadduct, as compared with that in pristine $Gd_3N@I_h(7)$-C_{80}. The planarization can be attributed to the release of the strain energy of the cluster by filling out the increased locally available endohedral space in the bisadduct. A portion of **14b** isomerized to **14a** under a thermal condition, although isomerization of another isomer as well as retrocycloaddition also proceeded simultaneously. The results indicated **14b** as a kinetic product, whereas the major bisadduct was a thermodynamic product. X-ray crystallographic identification of **14a** has been lacking. However, the authors proposed that **14a** also possesses a [6,6][6,6]-structure, although several candidates have similar relative stabilities. They also proposed that the isomerization can proceed via a "walk on the sphere" rearrangement, as observed in bis-malonate adducts of C_{60} under electrochemical conditions [52]. It is noteworthy that the two addition sites in the proposed structure of **14a** are the same as those in **13a**. At present, only the major products have been characterized while characterization of other minor products has been lacking. Future efforts will be devoted to the characterization of minor products to compare the regioselectivity in Bingel vs. 1,3-dipolar cycloadducts for EMFs and empty fullerenes.

5. Single-Bonding Derivatization of EMFs

When an odd number of electrons are formally transferred from the internal metal species to the carbon cages, the EMFs possess an open-shell electronic state. Such open-shell EMFs are stabilized by the delocalization of the unpaired electron over the molecule. The chemical reactivity of open-shell EMFs has also been explored [8]. Results have revealed that several reactions of open-shell EMFs, particularly those involving radical species, afforded singly bonded derivatives bearing a closed-shell electronic state [53–56]. Such single-bonding derivatization ability yielding closed-shell products is apparently a general trend for open-shell EMFs, such as trivalent M@C_{82}. In related work, we found that an open-shell EMF, Ce@C_{2v}(9)-C_{82}, was dimerized in its cocrystals with nickel octaethylporphyrin [57]. Similar dimerization was also apparent in the cocrystals of Y@C_s(6)-C_{82} [58] and Er@C_s(6)-C_{82} [59] with nickel octaethylporphyrin. In addition, functionalized EMFs bearing open-shell electronic species, such as La@C_{2v}(9)-C_{82}[$CH(CO_2Et)_2$]$_2$ [60] and La@C_{2v}(9)-C_{82}(Cp*) (Cp* = 1,2,3,4,5-pentamethylcyclopentadiene) [61], were dimerized in their crystals. In stark contrast, the monoaddition of a radical to closed-shell EMFs can yield fullerenyl radicals. In fact, the corresponding C_{60}-based fullerenyl radical R-C_{60}• can be generated by nucleophilic addition and subsequent one-electron oxidation, or by thermal dissociation of single-bonded fullerene dimers [62]. However, fullerenyl radicals are usually very reactive. They cannot be isolated because of their high radical reactivity. The results of the EPR studies suggest that an unpaired electron was not delocalized over the carbon sphere, but rather confined to the carbon at ortho and the two carbon atoms para to the sp^3-hybridized cage carbon bound with R in R-C_{60}•.

By contrast, we discovered, in 2015, that the monoaddition of a radical to a closed-shell EMF, La_2@I_h(7)-C_{80}, afforded a singly bonded fullerenyl radical as an air-stable product, as shown in Figure 5a [63]. The fullerenyl radical, La_2@I_h(7)-C_{80}–$C_3N_3Ph_2$ (**15**), was synthesized by the thermal reaction of La_2@I_h(7)-C_{80} and excess amount of 3-chloro-5,6-diphenyltriazine, under reflux in 1,2-DCB. The product was readily isolated by preparative HPLC. Subsequently, XRD analysis showed that the addition of the carbon-centered triazinyl radical took place at one of the carbon atoms shared by one pentagon and two hexagon rings, i.e., [5,6,6]-carbon atoms. The absorption spectrum of **15** exhibits broad absorption bands over the near-IR region down to 1300 nm, as a consequence of the paramagnetic nature. At this point, no meaningful NMR spectra were observed in **15**. The paramagnetic character was confirmed from X-band EPR measurements, showing that the EPR spectrum of **15** resembled that of La_2@I_h(7)-C_{80} anion radical. Detailed analysis revealed that a large spin density is associated with each La atom, and that each La atom has the same spin density. In fact, the LUMO of La_2@I_h(7)-C_{80} is well-known to be associated with the La–La σ-bonding orbital [64,65]. In this context, it is reasonable to state that the unusual stability of the fullerenyl radical in air arises from the confinement of the unpaired electron to an internal, metal–metal bonding orbital. The short La–La distance of 3.78 Å found in the crystal structure of the fullerenyl radical is consistent with this consideration. The chemical reactivity of the fullerenyl radical was also investigated. In fact, heating of the mixture of **15** and an excess amount of toluene in 1,2-DCB afforded addition of a benzyl to yield a closed-shell product, La_2@I_h(7)-C_{80}–($C_3N_3Ph_2$)(CH_2Ph) (**16**), in a 1,4-addition form. The product shows no EPR signals in solution due to the diamagnetic character. In addition, the longest absorption band was red-shifted in the absorption spectrum of **16** in solution, when compared with that of **15**. It is particularly interesting that this closed-shell product formed the open-shell dimer in its crystal. In this dimer, each unpaired electron is again confined to an internal La–La bonding orbital of each La_2@I_h(7)-C_{80} unit, to be a diradical. In fact, a broad signal was observed in the EPR spectrum of the crystal.

Triggered by this success, several groups have prepared and characterized similar fullerenyl radical derivatives of M_2@I_h(7)-C_{80} (hereinafter, the molecules are abbreviated as M_2@C_{80}). Lu et al. synthesized a benzyl derivative of La_2@C_{80} by the photochemical reaction of La_2@C_{80} with benzyl bromide in toluene; they have reported the short La–La distance (3.68–3.78 Å) in its crystal, as found in the crystal of **15** [66]. Later, Popov et al. also synthesized similar air-stable benzyl monoadducts of Y_2@ C_{80} and Dy_2@C_{80} by the reaction of the fullerene mixtures containing M_2@C_{80} (M = Y, Dy)

in DMF with benzyl bromide in 2017, as shown in Figure 5b [67]. They showed that giant exchange interactions between lanthanide ions and the unpaired electron caused single-molecule magnetism of $Dy_2@C_{80}(CH_2Ph)$, with a record-high 100 s blocking temperature of 18 K, and a high thermal barrier of magnetization reversal of 613 K. Subsequent surveys of an array of $M_2@C_{80}(CH_2Ph)$ (M_2 = Y_2, Gd_2, Tb_2, Dy_2, Ho_2, Er_2, TbY, TbGd) revealed that the strong ferromagnetic coupling emerging from the delocalization of the unpaired electron spin, which glues the magnetic moments of the two lanthanide ions together, is responsible for the high-spin magnetic ground states in the singly bonded derivatives [68]. Particularly, $Tb_2@C_{80}(CH_2Ph)$ showed giant coercivity and the highest known blocking temperature among dinuclear lanthanide complexes [69,70]. Additionally, they showed singly bonded derivatives. These derivatives are redox-active. Moreover, reversible one-electron oxidation and one-electron reduction were observed in their cyclic voltammograms, indicating that the single-molecule magnetism can be tuned electrochemically, as shown in Figure 5c.

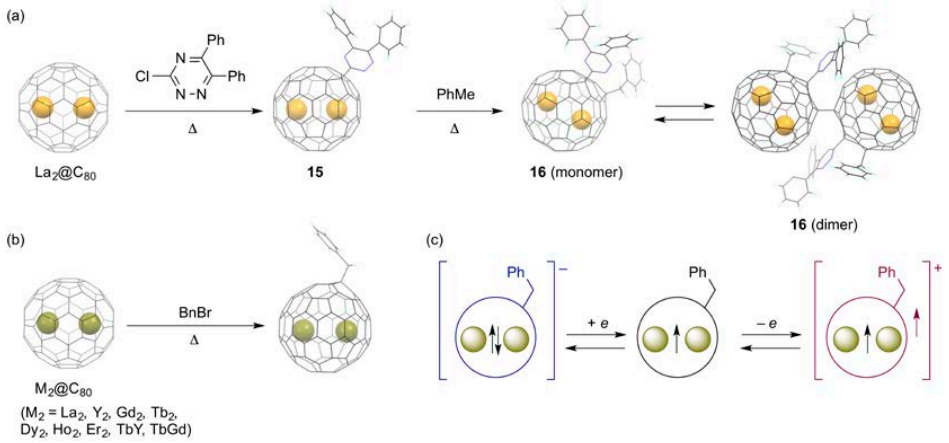

Figure 5. (**a**) Reaction of $La_2@C_{80}$ with 3-chloro-5,6-diphenyltriazine, and reaction of **15** with toluene. (**b**) Benzylation of $M_2@C_{80}$. (**c**) Schematic description of the single-electron reduction and oxidation of $M_2@C_{80}(CH_2Ph)$.

In 2011, Bazan and coworkers demonstrated that empty fullerenes such as C_{60} and C_{70} can behave as all carbon π-Lewis acids when combined with *N*-heterocyclic carbene (NHC) as counterparts [71]. Their results showed that a singly bonded C_{60} derivative bearing a strong zwitterionic character was obtained as a Lewis acid–base adduct. In this context, the chemical reactivity of EMFs toward NHCs has been attracting growing interest to elucidate the π-Lewis acidity of the negatively charged EMF carbon cages [72]. Lu et al. reported the that reaction of $Sc_3N@C_{80}$ with 1,3-bis(diisopropylphenyl)-imidazol-2-ylene (IDipp) afforded a singly bonded derivative, [6,6,6]-$Sc_3N@I_h(7)$-C_{80}-IDipp (**17**) [73]. In addition, the XRD analysis of **17** demonstrated that the NHC bonded to the $Sc_3N@C_{80}$ cage with its "abnormal" carbene center C5, instead of the normal site C2, which differs from the corresponding C_{60}–IDipp adduct, as shown in Figure 6a. Subsequent DFT calculations suggested that the formation of the [6,6,6]-adduct was not a thermodynamically controlled process. It is particularly interesting that introducing a small amount of oxygen in the reaction mixture induces formation of different products. In fact, the reaction of $M_3N@C_{80}$ (M = Sc, Lu) with IDipp in the presence of oxygen afforded not only the C5-linked [6,6,6]-$M_3N@C_{80}$-IDipp, but also the oxidized derivative of C2-linked [6,6,6]-$M_3N@C_{80}$-IDipp (**18**) [74]. It is proposed that the addition of oxygen can release the steric hindrance between the bulky NHC moiety and the EMF cage.

The reactivity of NHCs toward EMFs depends on the bulkiness of the substituents of NHC as well as on the cage structure and the encapsulated species of EMFs used. For instance, the reaction of $Sc_2C_2@C_{3v}(8)$-C_{82} with IDipp in the absence of oxygen proceeded regioselectively, to afford two products [75]. Subsequent XRD analysis of one product showed that the product is a singly bonded derivative, [5,6,6]-$Sc_2C_2@C_{3v}(8)$-C_{82}-IDipp, in which IDipp is linked to the EMF cage with its

normal carbon center C2. In contrast, the reaction of $Lu_2@C_{82}$ species (C_{82} = C_{3v}(8)-C_{82}, C_{2v}(9)-C_{82}) with 3-dimesityl-1*H*-imidazol-3-ium-2-ide (IMes) in the presence of oxygen afforded C2-linked [5,6,6]-$Lu_2@C_{82}$-IMes as a single product without formation of any oxidized product [76]. These results suggest that the high regioselectivity and preferential formation for monoadducts are determined mainly by the electronic effect of the EMF carbon cages and the steric repulsion between the NHC and EMFs. In fact, DFT calculations suggest that the coverage of the cage carbons featuring both large LUMO distribution and positive electrostatic potential values by the bulky NHC group can engender prevention of further additions. In contrast to the reactivity of NHCs, the reactions of *S*-heterocyclic carbenes (SHCs), generated in situ by the cycloaddition of disilenes and digermenes to CS_2 with $Sc_3N@I_h(7)$-C_{80}, afforded the corresponding methano-bridged derivatives (**19a,b**), as shown in Figure 6b [77]. Although the XRD characterization is lacking, NMR spectral analyses suggest that these derivatives possess the corresponding [6,6]-open structures.

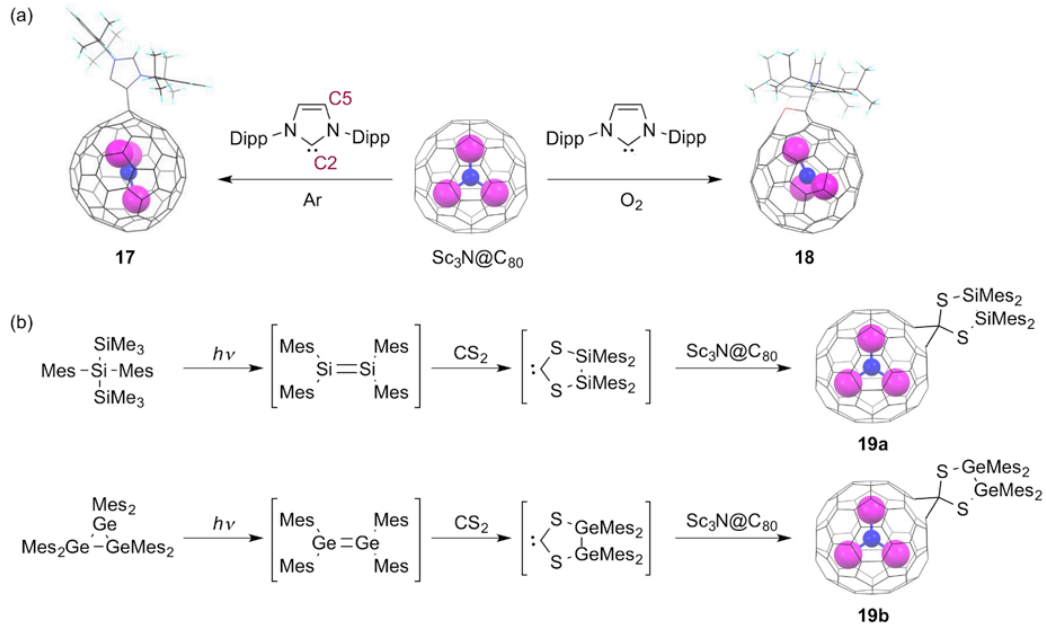

Figure 6. (**a**) Reactions of $Sc_3N@C_{80}$ with 1,3-bis(diisopropylphenyl)-imidazol-2-ylene in the absence or presence of oxygen. (**b**) Reactions of $Sc_3N@C_{80}$ with in situ generated SHCs.

6. Summary

This review has highlighted the unique chemical reactivity of EMFs, which differs from that of empty fullerenes. The structural diversity of EMFs has provided extreme variation in chemical reactivities. The resulting derivatives exhibited interesting properties derived from the combination of the cage structures, encaged metal species, and the functional groups bonded to the carbon cages. For instance, recent results have demonstrated clearly that the site of addition in the carbon cage is governed by metal-atom doping. This is also the case for the second addition. Particularly, the location of the internal metal atoms strongly affects the site-selectivity of EMFs. Selective bisfunctionalization of EMFs is expected to be valuable for the construction of EMF-based functional materials. In this respect, further efforts are anticipated to address selective trisfunctionalization using the triangular structures of trimetallic nitride clusters. Cage opening of EMFs to modulate the internal, untouchable metal species has remained challenging. However, recent studies of this aspect have led to remarkable progress in the first step of the molecular surgery of EMFs. The discovery of air-stable EMF-based fullerenyl radicals featuring confinement of an unpaired electron on the internal orbital paves the way to EMF-based single molecular magnets bearing giant exchange interactions. In addition, exploring the use of the π-Lewis acidity of EMF carbon cages by combining with heterocyclic carbenes provides

novel zwitterionic EMF derivatives. Studies of EMFs will continue to gain importance in achieving the construction of multifunctional molecules for applications.

Funding: This work was supported by Grants-in-Aid for Scientific Research (C) (Nos. 20K05472, 20K05469) from the Ministry of Education, Culture, Sports, Science, and Technology of Japan.

Conflicts of Interest: The authors have no conflict of interest to declare.

References

1. Heath, J.R.; O'Brien, S.C.; Zhang, Q.; Liu, Y.; Curl, R.F.; Kroto, H.W.; Tittel, F.K.; Smalley, R.E. Lanthanum complexes of spheroidal carbon shells. *J. Am. Chem. Soc.* **1985**, *107*, 7779–7780. [CrossRef]
2. Shinohara, H. Endohedral metallofullerenes. *Rep. Prog. Phys.* **2000**, *63*, 843–892. [CrossRef]
3. Akasaka, T.; Nagase, S. *Endofullerenes: A New Family of Carbon Clusters*; Kluwer: Dordrecht, The Netherlands, 2002.
4. Dunsch, L.; Yang, S. Metal nitride cluster fullerenes: Their current state and future prospects. *Small* **2007**, *3*, 1298–1320. [CrossRef] [PubMed]
5. Chaur, M.N.; Melin, F.; Ortiz, A.L.; Echegoyen, L. Chemical, electrochemical, and structural properties of endohedral metallofullerenes. *Angew. Chem. Int. Ed.* **2009**, *48*, 7514–7538. [CrossRef] [PubMed]
6. Lu, X.; Feng, L.; Akasaka, T.; Nagase, S. Current status and future developments of endohedral metallofullerenes. *Chem. Soc. Rev.* **2012**, *41*, 7723–7760. [CrossRef]
7. Popov, A.A.; Yang, S.; Dunsch, L. Endohedral fullerenes. *Chem. Rev.* **2013**, *113*, 5989–6113. [CrossRef]
8. Nagase, S. Theory and calculations of molecules containing heavier main group elements and fullerenes encaging transition metals: Interplay with experiment. *Bull. Chem. Soc. Jpn.* **2014**, *87*, 167–195. [CrossRef]
9. Yamada, M.; Akasaka, T. Emergence of highly elaborated π-space and extending its functionality based on nanocarbons: New vistas in the fullerene world. *Bull. Chem. Soc. Jpn.* **2014**, *87*, 1289–1314. [CrossRef]
10. Jin, P.; Li, Y.; Magagula, S.; Chen, Z. Exohedral functionalization of endohedral metallofullerenes: Interplay between inside and outside. *Coord. Chem. Rev.* **2019**, *388*, 406–439. [CrossRef]
11. Wang, T.; Wang, C. Functional metallofullerene materials and their applications in nanomedicine, magnetics, and electronics. *Small* **2019**, *15*, 1901522. [CrossRef] [PubMed]
12. Rivera-Nazario, D.M.; Pinzón, J.R.; Stevenson, S.; Echegoyen, L.A. Buckyball maracas: Exploring the inside and outside properties of endohedral fullerenes. *J. Phys. Org. Chem.* **2013**, *26*, 194–205. [CrossRef]
13. Rodríguez-Fortea, A.; Balch, A.L.; Poblet, J.M. Endohedral metallofullerenes: A unique host-guest association. *Chem. Soc. Rev.* **2011**, *40*, 3551–3563. [CrossRef] [PubMed]
14. Kako, M.; Nagase, S.; Akasaka, T. Functionalization of endohedral metallofullerenes with reactive silicon and germanium compounds. *Molecules* **2017**, *22*, 1179. [CrossRef]
15. Kroto, H.W. The stability of the fullerenes C_n, with n = 24, 28, 32, 36, 50, 60 and 70. *Nature* **1987**, *329*, 529–531. [CrossRef]
16. Yamada, M.; Kurihara, H.; Suzuki, M.; Guo, J.S.; Waelchli, M.; Olmstead, M.M.; Balch, A.L.; Nagase, S.; Maeda, Y.; Hasegawa, T.; et al. $Sc_2@C_{66}$ Revisited: An endohedral fullerene with scandium ions nestled within two unsaturated linear triquinanes. *J. Am. Chem. Soc.* **2014**, *136*, 7611–7614. [CrossRef]
17. Yamada, M.; Akasaka, T.; Nagase, S. Salvaging reactive fullerenes from soot by exohedral derivatization. *Angew. Chem. Int. Ed.* **2018**, *57*, 13394–13405. [CrossRef]
18. Kikuchi, K.; Nakahara, N.; Wakabayashi, T.; Suzuki, S.; Shiromaru, H.; Miyake, Y.; Saito, K.; Ikemoto, I.; Kainosho, M.; Achiba, Y. NMR characterization of isomers of C_{78}, C_{82} and C_{84} fullerenes. *Nature* **1992**, *357*, 142–145. [CrossRef]
19. Dennis, T.J.S.; Shinohara, H. Isolation and characterization of the two major isomers of [84]Fullerene (C_{84}). *Chem. Commun.* **1998**, 619–620. [CrossRef]
20. Fowler, P.; Manolopoulos, D.E. *An Atlas of Fullerenes*; Clarendon Press: Oxford, UK, 1995.
21. Wang, C.-R.; Inakuma, M.; Shinohara, H. Metallofullerenes $Sc_2@C_{82}$(I,II) and $Sc_2@C_{86}$(I,II): Isolation and spectroscopic studies. *Chem. Phys. Lett.* **1999**, *300*, 379–384. [CrossRef]
22. Wang, C.-R.; Kai, T.; Tomiyama, T.; Yoshida, T.; Kobayashi, Y.; Nishibori, E.; Takata, M.; Sakata, M.; Shinohara, H. A scandium carbide endohedral metallofullerene: $(Sc_2C_2)@C_{84}$. *Angew. Chem. Int. Ed.* **2001**, *40*, 397–399. [CrossRef]

23. Yamazaki, Y.; Nakajima, K.; Wakahara, T.; Tsuchiya, T.; Ishitsuka, M.O.; Maeda, Y.; Akasaka, T.; Waelchli, M.; Mizorogi, N.; Nagase, S. Observation of ^{13}C NMR chemical shifts of metal carbides encapsulated in fullerenes: $Sc_2C_2@C_{82}$, $Sc_2C_2@C_{84}$, and $Sc_3C_2@C_{80}$. *Angew. Chem. Int. Ed.* **2008**, *47*, 7905–7908. [CrossRef] [PubMed]
24. Yamada, M.; Tanabe, Y.; Dang, J.-S.; Sato, S.; Mizorogi, N.; Hachiya, M.; Suzuki, M.; Abe, T.; Kurihara, H.; Maeda, Y.; et al. D_{2d}(23)-C_{84} versus $Sc_2C_2@D_{2d}$(23)-C_{84}: Impact of endohedral Sc_2C_2 doping on chemical reactivity in the photolysis of diazirine. *J. Am. Chem. Soc.* **2016**, *138*, 16523–16532. [CrossRef]
25. Bonneau, R.; Liu, M.T.H. Quantum yield of formation of diazo compounds from the photolysis of diazirines. *J. Am. Chem. Soc.* **1996**, *118*, 7229–7230. [CrossRef]
26. Hummelen, J.C.; Prato, M.; Wudl, F. There is a hole in my bucky. *J. Am. Chem. Soc.* **1995**, *117*, 7003–7004. [CrossRef]
27. Komatsu, K.; Murata, M.; Murata, Y. Encapsulation of molecular hydrogen in fullerene C_{60} by organic synthesis. *Science* **2005**, *307*, 238–240. [CrossRef] [PubMed]
28. Maroto, E.E.; Izquierdo, M.; Murata, M.; Filippone, S.; Komatsu, K.; Murata, Y.; Martin, N. Catalytic stereodivergent functionalization of $H_2@C_{60}$. *Chem. Commun.* **2014**, *50*, 740–742. [CrossRef]
29. Kurotobi, K.; Murata, Y. A single molecule of water encapsulated in fullerene C_{60}. *Science* **2011**, *333*, 613–616. [CrossRef]
30. Maroto, E.E.; Mateos, J.; Garcia-Borràs, M.; Osuna, S.; Filippone, S.; Herranz, M.Á.; Murata, Y.; Solà, M.; Martín, N. Enantiospecific *cis-trans* Isomerization in chiral fulleropyrrolidines: Hydrogen-bonding assistance in the carbanion stabilization in $H_2O@C_{60}$. *J. Am. Chem. Soc.* **2015**, *137*, 1190–1197. [CrossRef]
31. Krachmalnicoff, A.; Bounds, R.; Mamone, S.; Alom, S.; Concistre, M.; Meier, B.; Kouril, K.; Light, M.E.; Johnson, M.R.; Rols, S.; et al. The dipolar endofullerene $HF@C_{60}$. *Nat. Chem.* **2016**, *8*, 953–957. [CrossRef]
32. Vidal, S.; Izquierdo, M.; Alom, S.; Garcia-Borràs, M.; Filippone, S.; Osuna, S.; Solà, M.; Whitby, R.J.; Martín, N. Effect of incarcerated HF on the exohedral chemical reactivity of $HF@C_{60}$. *Chem. Commun.* **2017**, *53*, 10993–10996. [CrossRef]
33. Bloodworth, S.; Sitinova, G.; Alom, S.; Vidal, S.; Bacanu, G.R.; Elliott, S.J.; Light, M.E.; Herniman, J.M.; Langley, G.J.; Levitt, M.H.; et al. First synthesis and characterization of $CH_4@C_{60}$. *Angew. Chem. Int. Ed.* **2019**, *58*, 5038–5043. [CrossRef] [PubMed]
34. Wang, G.-W.; Liu, T.-X.; Jiao, M.; Wang, N.; Zhu, S.-E.; Chen, C.; Yang, S.; Bowles, F.L.; Beavers, C.M.; Olmstead, M.M.; et al. The cycloaddition reaction of I_h-$Sc_3N@C_{80}$ with 2-Amino-4,5-diisopropoxybenzoic acid and isoamyl nitrite to produce an open-cage metallofullerene. *Angew. Chem. Int. Ed.* **2011**, *50*, 4658–4662. [CrossRef] [PubMed]
35. Yamada, M.; Muto, Y.; Kurihara, H.; Slanina, Z.; Suzuki, M.; Maeda, Y.; Rubin, Y.; Olmstead, M.M.; Balch, A.L.; Nagase, S.; et al. Regioselective cage opening of $La_2@D_2$(10611)-C_{72} with 5,6-Diphenyl 3-(2-pyridyl)-1,2,4-triazine. *Angew. Chem. Int. Ed.* **2015**, *54*, 2232–2235. [CrossRef] [PubMed]
36. Kato, H.; Taninaka, A.; Sugai, T.; Shinohara, H. Structure of a missing-caged metallofullerene: $La_2@C_{72}$. *J. Am. Chem. Soc.* **2003**, *125*, 7782–7783. [CrossRef] [PubMed]
37. Lu, X.; Nikawa, H.; Nakahodo, T.; Tsuchiya, T.; Ishitsuka, M.O.; Maeda, Y.; Akasaka, T.; Toki, M.; Sawa, H.; Slanina, Z.; et al. Chemical understanding of a non-IPR metallofullerene: Stabilization of encaged metals on fused-pentagon bonds in $La_2@C_{72}$. *J. Am. Chem. Soc.* **2008**, *130*, 9129–9136. [CrossRef]
38. Lu, X.; Nikawa, H.; Tsuchiya, T.; Maeda, Y.; Ishitsuka, M.O.; Akasaka, T.; Toki, M.; Sawa, H.; Slanina, Z.; Mizorogi, N.; et al. Bis-carbene adducts of non-IPR $La_2@C_{72}$: Localization of high reactivity around fused pentagons and electrochemical properties. *Angew. Chem. Int. Ed.* **2008**, *47*, 8642–8645. [CrossRef]
39. Akasaka, T.; Nagase, S.; Kobayashi, K.; Wälchli, M.; Yamamoto, K.; Funasaka, H.; Kako, M.; Hoshino, T.; Erata, T. ^{13}C and ^{139}La NMR studies of $La_2@C_{80}$: First evidence for circular motion of metal atoms in endohedral dimetallofullerenes. *Angew. Chem. Int. Ed.* **1997**, *36*, 1643–1645. [CrossRef]
40. Ishitsuka, M.O.; Sano, S.; Enoki, H.; Sato, S.; Nikawa, H.; Tsuchiya, T.; Slanina, Z.; Mizorogi, N.; Liu, M.T.H.; Akasaka, T.; et al. Regioselective bis-functionalization of endohedral dimetallofullerene, $La_2@C_{80}$: Extremal La–La distance. *J. Am. Chem. Soc.* **2011**, *133*, 7128–7134. [CrossRef]
41. Yamada, M.; Someya, C.; Wakahara, T.; Tsuchiya, T.; Maeda, Y.; Akasaka, T.; Yoza, K.; Horn, E.; Liu, M.T.H.; Mizorogi, N.; et al. Metal atoms collinear with the spiro carbon of 6,6-open adducts, $M_2@C_{80}$(Ad) (M = La and Ce, Ad = Adamantylidene). *J. Am. Chem. Soc.* **2008**, *130*, 1171–1176. [CrossRef]
42. Cai, T.; Xu, L.; Shu, C.; Champion, H.A.; Reid, J.E.; Anklin, C.; Anderson, M.R.; Gibson, H.W.; Dorn, H.C. Selective formation of a symmetric $Sc_3N@C_{78}$ bisadduct: Adduct docking controlled by an internal trimetallic nitride cluster. *J. Am. Chem. Soc.* **2008**, *130*, 2136–2137. [CrossRef]

43. Yamada, M.; Abe, T.; Saito, C.; Yamazaki, T.; Sato, S.; Mizorogi, N.; Slanina, Z.; Uhlik, F.; Suzuki, M.; Maeda, Y.; et al. Adamantylidene addition to $M_3N@I_h$-C_{80} (M = Sc, Lu) and $Sc_3N@D_{5h}$-C_{80}: Synthesis and crystallographic characterization of the [5,6]-open and [6,6]-open adducts. *Chem. Eur. J.* **2017**, *23*, 6552–6561. [CrossRef] [PubMed]
44. Maggini, M.; Scorrano, G.; Prato, M. Addition of azomethine ylides to C_{60}: Synthesis, characterization, and functionalization of fullerene pyrrolidines. *J. Am. Chem. Soc.* **1993**, *115*, 9798–9799. [CrossRef]
45. Cardona, C.M.; Kitaygorodskiy, A.; Ortiz, A.; Herranz, M.Á.; Echegoyen, L. The First Fulleropyrrolidine derivative of $Sc_3N@C_{80}$: Pronounced chemical shift differences of the geminal protons on the pyrrolidine ring. *J. Org. Chem.* **2005**, *70*, 5092–5097. [CrossRef] [PubMed]
46. Cardona, C.M.; Kitaygorodskiy, A.; Echegoyen, L. Trimetallic nitride endohedral metallofullerenes: Reactivity dictated by the encapsulated metal cluster. *J. Am. Chem. Soc.* **2005**, *127*, 10448–10453. [CrossRef]
47. Cai, T.; Ge, Z.; Iezzi, E.B.; Glass, T.E.; Harich, K.; Gibson, H.W.; Dorn, H.C. Synthesis and characterization of the first trimetallic nitride templated pyrrolidino endohedral metallofullerenes. *Chem. Commun.* **2005**, 3594–3596. [CrossRef]
48. Cai, T.; Slebodnick, C.; Xu, L.; Harich, K.; Glass, T.E.; Chancellor, C.; Fettinger, J.C.; Olmstead, M.M.; Balch, A.L.; Gibson, H.W.; et al. A Pirouette on a metallofullerene sphere: Interconversion of isomers of N-Tritylpyrrolidino I_h $Sc_3N@C_{80}$. *J. Am. Chem. Soc.* **2006**, *128*, 6486–6492. [CrossRef]
49. Pinzón, J.R.; Plonska-Brzezinska, M.E.; Cardona, C.M.; Athans, A.J.; Gayathri, S.S.; Guldi, D.M.; Herranz, M.Á.; Martín, N.; Torres, T.; Echegoyen, L. $Sc_3N@C_{80}$-ferrocene electron-donor/acceptor conjugates as promising materials for photovoltaic applications. *Angew. Chem. Int. Ed.* **2008**, *47*, 4173–4176. [CrossRef]
50. Semivrazhskaya, O.; Romero-Rivera, A.; Aroua, S.; Troyanov, S.I.; Garcia-Borràs, M.; Stevenson, S.; Osuna, S.; Yamakoshi, Y. Structures of $Gd_3N@C_{80}$ prato bis-adducts: Crystal structure, thermal isomerization, and computational study. *J. Am. Chem. Soc.* **2019**, *141*, 10988–10993. [CrossRef]
51. Aroua, S.; Garcia-Borràs, M.; Bölter, M.F.; Osuna, S.; Yamakoshi, Y. Endohedral metal-induced regioselective formation of bis-prato adduct of $Y_3N@I_h$-C_{80} and $Gd_3N@I_h$-C_{80}. *J. Am. Chem. Soc.* **2015**, *137*, 58–61. [CrossRef]
52. Kessinger, R.; Gomez-Lopez, M.; Boudon, C.; Gisselbrecht, J.-P.; Gross, M.; Echegoyen, L.; Diederich, F. Walk on the Sphere: Electrochemically Induced Isomerization of C_{60} Bisadducts by migration of di(alkoxycarbonyl)methano bridges. *J. Am. Chem. Soc.* **1998**, *120*, 8545–8546. [CrossRef]
53. Feng, L.; Nakahoto, T.; Wakahara, T.; Tsuchiya, T.; Maeda, Y.; Akasaka, T.; Kato, T.; Horn, E.; Yoza, K.; Mizorogi, N.; et al. A singly bonded derivative of endohedral metallofullerene: $La@C_{82}CBr(COOC_2H_5)_2$. *J. Am. Chem. Soc.* **2005**, *127*, 17136–17137. [CrossRef] [PubMed]
54. Takano, Y.; Yomogida, A.; Nikawa, H.; Yamada, M.; Wakahara, T.; Tsuchiya, T.; Ishitsuka, M.O.; Maeda, Y.; Akasaka, T.; Kato, T.; et al. Radical coupling reaction of paramagnetic endohedral metallofullerene $La@C_{82}$. *J. Am. Chem. Soc.* **2008**, *130*, 16224–16230. [CrossRef] [PubMed]
55. Takano, Y.; Tasita, R.; Suzuki, M.; Nagase, S.; Imahori, H.; Akasaka, T. Molecular location sensing approach by anisotropic magnetism of an endohedral metallofullerene. *J. Am. Chem. Soc.* **2016**, *138*, 8000–8006. [CrossRef] [PubMed]
56. Fang, H.; Cong, H.; Suzuki, M.; Bao, L.; Yu, B.; Xie, Y.; Mizorogi, N.; Olmstead, M.M.; Balch, A.L.; Nagase, S.; et al. Regioselective benzyl radical addition to an open-shell cluster metallofullerene. crystallographic studies of cocrystallized $Sc_3C_2@I_h$-C_{80} and its singly bonded derivative. *J. Am. Chem. Soc.* **2014**, *136*, 10534–10540. [CrossRef]
57. Suzuki, M.; Yamada, M.; Maeda, Y.; Sato, S.; Takano, Y.; Uhlik, F.; Slanina, Z.; Lian, Y.; Lu,, X.; Nagase, S.; et al. The unanticipated dimerization of $Ce@C_{2v}(9)$-C_{82} upon co-crystallization with Ni(octaethylporphyrin) and comparison with monomeric $M@C_{2v}(9)$-C_{82} (M = La, Sc, and Y). *Chem. Eur. J.* **2016**, *22*, 18115–18122. [CrossRef]
58. Bao, L.; Pan, C.; Slanina, Z.; Uhlik, F.; Akasaka, T.; Lu, X. Isolation and crystallographic characterization of the labile isomer of $Y@C_{82}$ Cocrystallized with Ni(OEP): Unprecedented dimerization of pristine metallofullerenes. *Angew. Chem. Int. Ed.* **2016**, *55*, 9234–9238. [CrossRef]
59. Hu, S.; Liu, T.; Shen, W.; Slanina, Z.; Akasaka, T.; Xie, Y.; Uhlik, F.; Huang, W.; Lu, X. Isolation and structural characterization of $Er@C_{2v}(9)$-C_{82} and $Er@C_s(6)$-C_{82}: Regioselective dimerization of a pristine endohedral metallofullerene induced by cage symmetry. *Inorg. Chem.* **2019**, *58*, 2177–2182. [CrossRef]
60. Feng, L.; Tsuchiya, T.; Wakahara, T.; Nakahodo, T.; Piao, Q.; Maeda, Y.; Akasaka, T.; Kato, T.; Yoza, K.; Horn, E.; et al. Synthesis and characterization of a bisadduct of $La@C_{82}$. *J. Am. Chem. Soc.* **2006**, *128*, 5990–5991. [CrossRef]

61. Maeda, Y.; Sato, S.; Inada, K.; Nikawa, H.; Yamada, M.; Mizorogi, N.; Hasegawa, T.; Tsuchiya, T.; Akasaka, T.; Kato, T.; et al. Regioselective exohedral functionalization of La@C_{82} and its 1,2,3,4,5-pentamethylcyclopentadiene and adamantylidene adducts. *Chem. Eur. J.* **2010**, *16*, 2193–2197. [CrossRef]
62. Tzirakis, M.D.; Orfanopoulos, M. Radical reactions of fullerenes: From synthetic organic chemistry to materials science and technology. *Chem. Rev.* **2013**, *113*, 5262–5321. [CrossRef]
63. Yamada, M.; Kurihara, H.; Suzuki, M.; Saito, M.; Slanina, Z.; Uhlik, F.; Aizawa, T.; Kato, T.; Olmstead, M.M.; Balch, A.L.; et al. Hiding and recovering electrons in a dimetallic endohedral fullerene: Air-stable products from radical additions. *J. Am. Chem. Soc.* **2015**, *137*, 232–238. [CrossRef] [PubMed]
64. Suzuki, T.; Maruyama, Y.; Kato, T.; Kikuchi, K.; Nakao, Y.; Achiba, Y.; Kobayashi, K.; Nagase, S. Electrochemistry and ab initio study of the dimetallofullerene La_2@C_{80}. *Angew. Chem. Int. Ed. Engl.* **1995**, *34*, 1094–1096. [CrossRef]
65. Yamada, M.; Slanina, Z.; Mizorogi, N.; Muranaka, A.; Maeda, Y.; Nagase, S.; Akasaka, T.; Kobayashi, N. Application of MCD spectroscopy and TD-DFT to endohedral metallofullerenes for characterization of their electronic transitions. *Phys. Chem. Chem. Phys.* **2013**, *15*, 3593–3601. [CrossRef] [PubMed]
66. Bao, L.; Chen, M.; Pan, C.; Yamaguchi, T.; Kato, T.; Olmstead, M.M.; Balch, A.L.; Akasaka, T.; Lu, X. Crystallographic evidence for direct metal–metal bonding in a stable open-shell La_2@I_h-C_{80} derivative. *Angew. Chem. Int. Ed.* **2016**, *55*, 4242–4246. [CrossRef]
67. Liu, F.; Krylov, D.S.; Spree, L.; Avdoshenko, S.M.; Samoylova, N.A.; Rosenkranz, M.; Kostanyan, A.; Greber, T.; Wolter, A.U.B.; Buchner, B.; et al. Single molecule magnet with an unpaired electron trapped between two lanthanide ions inside a fullerene. *Nat. Commun.* **2017**, *8*, 16098. [CrossRef]
68. Liu, F.; Velkos, G.; Krylov, D.S.; Spree, L.; Zalibera, M.; Ray, R.; Samoylova, N.A.; Chen, C.-H.; Rosenkranz, M.; Schiemenz, S.; et al. Air-stable redox-active nanomagnets with lanthanide spins radical—bridged by a metal–metal bond. *Nat. Commun.* **2019**, *10*, 571. [CrossRef]
69. Liu, F.; Spree, L.; Krylov, D.S.; Velkos, G.; Avdoshenko, S.M.; Popov, A.A. Single-electron lanthanide-lanthanide bonds inside fullerenes toward robust redox-active molecular magnets. *Acc. Chem. Res.* **2019**, *52*, 2981–2993. [CrossRef]
70. Spree, L.; Popov, A.A. Recent advances in single molecule magnetism of dysprosium-metallofullerenes. *Dalton Trans.* **2019**, *48*, 2861–2871. [CrossRef]
71. Li, H.; Risko, C.; Seo, J.H.; Campbell, C.; Wu, G.; Brédas, J.-L.; Bazan, G.C. Fullerene–carbene lewis acid–base adducts. *J. Am. Chem. Soc.* **2011**, *133*, 12410–12413. [CrossRef]
72. Bao, L.; Peng, P.; Lu, X. Bonding inside and outside fullerene cages. *Acc. Chem. Res.* **2018**, *51*, 810–815. [CrossRef]
73. Chen, M.; Bao, L.; Ai, M.; Shen, W.; Lu, X. Sc_3N@I_h-C_{80} as a novel lewis acid to trap abnormal *n*-heterocyclic carbenes: The unprecedented formation of a singly bonded [6,6,6]-adduct. *Chem. Sci.* **2016**, *7*, 2331–2334. [CrossRef] [PubMed]
74. Chen, M.; Shen, W.; Peng, P.; Bao, L.; Zhao, S.; Xie, Y.; Jin, P.; Fang, H.; Li, F.-F.; Lu, X. Evidence of oxygen activation in the reaction between an *N*-heterocyclic carbene and M_3N@I_h(7)-C_{80}: An unexpected method of steric hindrance release. *J. Org. Chem.* **2017**, *82*, 3500–3505. [CrossRef] [PubMed]
75. Bao, L.; Chen, M.; Shen, W.; Yang, L.; Jin, P.; Lu, X. Lewis acid–base adducts of Sc_2C_2@C_{3v}(8)-C_{82}/N-Heterocyclic carbene: Toward isomerically pure metallofullerene derivatives. *Inorg. Chem.* **2017**, *56*, 14747–14750. [CrossRef] [PubMed]
76. Shen, W.; Yang, L.; Wu, Y.; Bao, L.; Li, Y.; Jin, P.; Fang, H.; Xie, Y.; Lu, X. Reactions between *N*-Heterocyclic carbene and lutetium–metallofullerenes: High regioselectivity directed by electronic effect in addition to steric hindrance. *J. Org. Chem.* **2019**, *84*, 606–612. [CrossRef]
77. Kako, M.; Arikawa, Y.; Kanzawa, S.; Yamada, M.; Maeda, Y.; Furukawa, M.; Akasaka, T. Addition of S-Heterocyclic carbenes to fullerenes: Formation and characterization of dithiomethano-bridged derivatives. *Helv. Chim. Acta* **2019**, *102*, e1900064. [CrossRef]